

EXPERIMENTAL STUDIES OF EXPLOSIVELY- DRIVEN MAGNETOHYDRODYNAMIC GENERATORS

**F. J. Agee
G. Baca
D. Chama
F. M. Lehr
T. Englert
J. Gaudet
D. Shiffler
M. Vigil
R. Kaye**

October 1997

Final Report

APPROVED FOR PUBLIC RELEASE; DISTRIBUTION IS UNLIMITED.



**AIR FORCE RESEARCH LABORATORY
Directed Energy Directorate
3550 Aberdeen Ave SE
AIR FORCE MATERIEL COMMAND
KIRTLAND AIR FORCE BASE, NM 87117-5776**


Using Government drawings, specifications, or other data included in this document for any purpose other than Government procurement does not in any way obligate the U.S. Government. The fact that the Government formulated or supplied the drawings, specifications, or other data, does not license the holder or any other person or corporation; or convey any rights or permission to manufacture, use, or sell any patented invention that may relate to them.

This report has been reviewed by the Public Affairs Office and is releasable to the National Technical Information Service (NTIS). At NTIS, it will be available to the general public, including foreign nationals.

If you change your address, wish to be removed from this mailing list, or your organization no longer employs the addressee, please notify AFRL/DEHE, 3550 Aberdeen Ave SE, Kirtland AFB, NM 87117-5776.


Do not return copies of this report unless contractual obligations or notice on a specific document requires its return.

This report has been approved for publication.




LEON J. CHANDLER, DR-III
Project Manager

FOR THE COMMANDER



ROBERT E. PETERKIN, DV-IV
Chief, Plasma Physics Branch



R. EARL GOOD, SES
Director, Directed Energy

REPORT DOCUMENTATION PAGE			Form Approved OMB No. 074-0188	
Public reporting burden for this collection of information is estimated to average 1 hour per response, including the time for reviewing instructions, searching existing data sources, gathering and maintaining the data needed, and completing and reviewing this collection of information. Send comments regarding this burden estimate or any other aspect of this collection of information, including suggestions for reducing this burden to Washington Headquarters Services, Directorate for Information Operations and Reports, 1215 Jefferson Davis Highway, Suite 1204, Arlington, VA 22202-4302, and to the Office of Management and Budget, Paperwork Reduction Project (0704-0188), Washington, DC 20503				
1. AGENCY USE ONLY (Leave blank)	2. REPORT DATE October 1997	3. REPORT TYPE AND DATES COVERED Final Report 01 October 94 – 31 October 97		
4. TITLE AND SUBTITLE Experimental Studies of Explosively-Driven Magnetohydrodynamic Generators		5. FUNDING NUMBERS PE: 62601F PR: 5797 TA: AK WU: 09		
6. AUTHOR(S) F. J. Agee, G. Baca, D. Chama, F. M. Lehr, T. Englert, J. Gaudet, D. Shiffler, M. Vigil and R. Kaye				
7. PERFORMING ORGANIZATION NAME(S) AND ADDRESS(ES) Air Force Research Laboratory 3550 Aberdeen Avenue, SE Kirtland, AFB, NM 87117-5776		8. PERFORMING ORGANIZATION REPORT NUMBER AFRL-DE-PS-TR-1998-1073		
9. SPONSORING / MONITORING AGENCY NAME(S) AND ADDRESS(ES)		10. SPONSORING / MONITORING AGENCY REPORT NUMBER		
11. SUPPLEMENTARY NOTES				
12a. DISTRIBUTION / AVAILABILITY STATEMENT Approved for public release; distribution is unlimited.			12b. DISTRIBUTION CODE	
13. ABSTRACT (<i>Maximum 200 Words</i>) The field of High Power Microwaves (HPM) has evolved as a result of advances in the field of pulsed power, which has made pulses of electrical energy available that can drive HPM sources to gigawatt levels. One of the most compact forms of pulsed power involves the storage of chemical energy in the form of explosive charges. Explosive magnetohydrodynamic (MHD) generators are electrical power sources, which convert the kinetic energy of moving plasma into useful electrical energy through the magnetic portion of the Lorentz force. This report describes research conducted by the Air Force Research Laboratory to test specific designs of explosively driven magnetohydrodynamic generators. The goal of the research was to investigate the use of gigawatt generators in driving reactive loads appropriate to diode, and ultimately HPM applications. Two test series were performed, the first of which consisted of experiments on a low voltage generator and the second of which had the goal of scaling the existing design to higher voltage while retaining the reactive-type load. The complex problem of diagnostics of the plasma in this explosive test was addressed using fast, temporally resolved, plasma measurements, as well as spectroscopic plasma constituent measurements.				
14. SUBJECT TERMS High power microwaves; explosive magnetohydrodynamic (MHD) generators; pulsed power; Power			15. NUMBER OF PAGES 42	
			16. PRICE CODE	
17. SECURITY CLASSIFICATION OF REPORT Unclassified	18. SECURITY CLASSIFICATION OF THIS PAGE Unclassified	19. SECURITY CLASSIFICATION OF ABSTRACT Unclassified	20. LIMITATION OF ABSTRACT UL	

TABLE OF CONTENTS

1. ABSTRACT.....	1
2. INTRODUCTION	1
3. THEORY OF OPERATION.....	3
4. EXPERIMENTAL CONFIGURATION	4
5. LOW VOLTAGE GENERATOR	6
5.1 Overview.....	6
5.2 Pre-Shot Predictions.....	6
5.3 Results.....	7
5.4 Discussion.....	8
6. HIGH VOLTAGE GENERATOR.....	9
6.1 Overview.....	9
6.2 Pre-Shot Predictions.....	10
6.3 Results.....	10
6.4 Discussion.....	11
7. CONCLUSIONS.....	14
8. ACKNOWLEDGMENT.....	15
REFERENCES	16

LIST OF FIGURES

1. Generalized geometry for the MHD generator experiments. Each generator design shared these common features.	20
2. Schematic of the low voltage generator. The view shows basic components of the generator without showing the electrical load. The explosive is detonated with an RP-2 detonator. The magnetic field is produced using the coils depicted in the drawing.	21
3. Equivalent circuit drawing for the generator and load used in the low voltage generator experiments. The resistance, R_i , is a variable parameter used to model the internal resistance of the generator.	22
4. Results of the circuit simulation showing the load voltage as function of time for the low voltage generator. It shows a family of curves with the generator impedance as a free parameter.	23
5. Load voltage and load current measured in the low voltage generator experiment, shot number 1. The peak voltage and current are 12.4 kV and 12.0 kA respectively.	24
6. Schematic showing the design of the high voltage generator. Note the similarities to the low voltage generator shown in Figure 2. The major difference in the two generators is in the geometry of the explosive driver and the amount of explosives used in the experiment.	25
7. Equivalent circuit drawing for the generator and load used in the high voltage generator experiments.	26
8. Predicted waveform for the load voltage in the high voltage generator experiment. Since the load impedance is large, the variation of the voltage and current is minor and hence a family of curves is not shown.	27
9. PIN signals from the high voltage generator experiments. The signals show the plasma arrival at various PIN positions along the shock tube.	28
10. Load voltage measured in the high voltage generator experiment.	29
11. Load current measured in the high voltage generator experiment.	30
12. Signal from the first optical fiber used to determine the rate of plasma flow. Light is detected using a photomultiplier tube with a monochromator tuned to 480.6 nm. The different slopes seen on the curve indicate distinct changes in the plasma wave front.	31
13. A re-plot of the data obtained from second optical fiber mounted along the shock tube. Average signal level is depicted. Light is detected using an avalanche photodiode coupled to a monochromator tuned to 480.6 nm. The probe position coincides with PIN #6.	32
14. Optical spectra obtained from the plasma propagating along the shock tube. The fibers are placed in sequence, at A = 15.24 cm (6.0 in.), B = 20.32 cm (8.0 in.), C = 25.4 cm (10.0 in.), and D = 30.48 cm (12.0 in.), measured from the explosive driver side of the shock tube. Arrows indicate position of Ar II line at 480.8 nm.	33

LIST OF TABLES

I. Overview of the experimental parameters for the low voltage tests.....	18
II. Key design features and predicted performance goals for the high voltage MHD generator.	19

1. ABSTRACT

The field of High Power Microwaves (HPM) has evolved as a result of advances in the field of pulsed power, which has made pulses of electrical energy available that can drive HPM sources to gigawatt levels. One of the most compact forms of pulsed power involves the storage of chemical energy in the form of explosive charges. Explosive magnetohydrodynamic (MHD) generators are electrical power sources which convert the kinetic energy of moving plasma into useful electrical energy through the magnetic portion of the Lorentz force. This report describes research conducted by the Air Force Phillips Laboratory to test specific designs of explosively-driven magnetohydrodynamic (EDMHD) generators. The goal of the research was to investigate the use of gigawatt generators in driving reactive loads appropriate to diode, and ultimately HPM applications. Two test series were performed, the first of which consisted of experiments on a low voltage generator and the second of which had the goal of scaling the existing design to higher voltage while retaining the reactive-type load. The complex problem of diagnostics of the plasma in this explosive test was addressed using fast, temporally-resolved, plasma measurements, as well as spectroscopic plasma constituent measurements.

2. INTRODUCTION

High Power Microwave (HPM) narrow band source research is focused today upon a number of issues that relate to the generation of multi-microsecond pulses of RF energy at power in excess of 1 GW. Pulsed power systems in the laboratory can provide pulses of relativistic electrons powerful enough to achieve these levels even for relatively inefficient sources such as vircators, reflex diodes and triodes, where the efficiency may be only a fraction of a percent [1], [2]. These powerful sources of pulsed electrical energy are large and heavy, and the search for compact pulsed power alternatives is an obvious adjunct to the search for efficient and compact HPM sources. The idea of using explosives to provide a compact electrical energy source has been studied in a number of laboratories for a variety of applications [3] – [5]. When considering the use of explosive pulsed power to drive HPM sources, the issue of having sufficient power is not challenging due to the very high energy density of chemical explosives. The chemical energy density of Composition C-4 used in these experiments reported here

was in the range of $10 - 20 \text{ kJ/cm}^3$. Furthermore, the pulsed waveforms from explosively driven pulsed power systems are much longer than required to meet or exceed the pulse duration of interest, as the pulses can easily be milliseconds long.

The principal problem associated with explosively-driven pulsed power for HPM applications is that the current produced, which can be in the range of thousands to millions of amperes, comes at very low impedance, typically a small fraction of an ohm. This is not suitable for HPM tubes. HPM tubes work at impedances ranging from a few ohms to more than 1000 ohms. For example, relativistic magnetrons operate at impedances from 20 to 200 ohms, relativistic traveling wave tubes (TWTs) and backward wave oscillators (BWOs) work at from 200 to 300 ohms, and relativistic klystrons work at impedances of 35 to 1700 ohms [6]. Consequently, the primary issue in explosive pulsed power is that of power conditioning to transform an inherently high current very low voltage source into a much higher voltage source.

There are a number of types of explosive pulsed power sources, including magnetohydrodynamic (MHD) generators and flux compression generators (FCGs). The latter have achieved energy in the range of 0.5 to 100 MJ and currents from 0.8 to over 300 MA, and have a relatively modest cost of $\$10^{-3}/\text{J}$ relative to the $\$1-\$2/\text{J}$ for conventional pulsed power sources [7]. They can also be designed to produce pulses in the 1 - 10 microsecond range, which is ideal for driving HPM tubes [8]. However, one serious disadvantage of flux compression generators that are very compact in size and lightweight is their extremely low impedance. Typical helical FCGs produce several 100s of kA of current at 10s of kV. Thus, the internal impedance of such devices can be as low as $1 - 10 \text{ m}\Omega$. MHD generators have an impedance which depends upon the shock tube (plasma channel) aspect ratio. The larger the aspect ratio (channel width/electrode separation) the larger the internal resistance of the generator [9].

This report discusses results of research performed to date on explosive MHD generators, which also have the potential for producing pulses suitable for driving HPM tubes. Explosive MHD generators are electrical power sources that convert the kinetic energy of a moving plasma into useful electrical energy through the magnetic force term of the Lorentz force law. These generators are capable of power outputs in the gigawatt range with pulse durations from the microsecond to the second time scales [9] –

[11]. Research was conducted by the Air Force Phillips Laboratory and Sandia National Laboratories (SNL) to test specific designs of explosively-driven magnetohydrodynamic (EDMHD) generators. The goal of the research was to investigate the use of gigawatt generators in driving reactive loads. Specifically, voltage waveforms obtained from an earlier design [12] were of particular interest because of the reported rise time (0.5 to 1.5 μ s) and the relatively flat top and pulse width of 1 – 2 μ s.

Two test series were performed. The first test series consisted of experiments using a low voltage generator [13] designed and tested by SNL under resistive load conditions only. The goal of these new experiments was to determine the interaction of the generator with a reactive load similar to the situation encountered with an HPM diode load. The SNL design chosen for this series of tests was design #6, the latest design of the compact explosively-driven MHD generator operating at a peak power of greater than 1 GW. Two separate shots were done using design #6 in the low voltage series. The second test series had the goal of scaling the existing design #6 to higher voltages while retaining the reactive load. Only one test was conducted successfully of the high voltage generator using this new design. One other test was attempted, but failed due to an explosive misfire.

This report describes the test results for both generator designs, the lower voltage generator and the new high voltage generator. The next section begins with a brief description of the theory of operation of explosively driven MHD generators. Then, the two series of experiments, calculations of performance, and results follow. First, the low voltage generators are described, followed by a discussion of the larger, high voltage generator experiment. The significance of these results is then discussed and concluding remarks are made.

3. THEORY OF OPERATION

MHD generators use the magnetic force applied to a moving plasma to extract energy from the bulk motion of the plasma. If an ionized gas is forced to enter a region of magnetic field, in general, this plasma will experience a force perpendicular to the motion of the gas and to the direction of the field. As a special case, if the plasma also moves perpendicular to the magnetic field in a region of space bounded by conductors, the voltage produced between the conductors by the induced charge separation

is equal to UBd , where U is the flow velocity, B is the external magnetic induction strength, and d separation distance between the electrodes. The open circuit voltage, V_{oc} , of the generator is, thus, given by:

$$V_{oc} = Ubd. \quad (1)$$

There are in general many factors that alter the simple behavior of the MHD generator. Some of these are: boundary layer formation that traps the external magnetic field lines and distorts them near the electrode surfaces; the formation of many species of partially and multiply ionized gases; 3D effects or geometry factors that alter the flow of the gas and the behavior of the EM fields; turbulent flow of the plasma as it enters the shock tube; and other plasma-related interactions. Despite these many factors which alter the basic relationship, it is instructive to use the simple theory to predict the generator's performance.

In order to analyze the detailed behavior of the two generator designs tested in these experiments, it is necessary to conduct computer modeling of the hydrodynamic flow in these geometries. To date, calculations using the CTH code [14] have been done on generator design #6 only. The modeling results done for these early designs were used to estimate the gas flow through the generator in the first series of tests with the low voltage generator (see pre-shot predictions discussed below). This was possible because the geometry of the generator and explosive driver used here was the same as for this previous research. No MHD calculations have been attempted due to the difficult numerical challenges involved with large Reynolds number problems at very late times (10's of μs) compared to the plasma dynamics [15]. Further, no CTH calculations were attempted for the high voltage generator design.

4. EXPERIMENTAL CONFIGURATION

A block diagram showing the generalized geometry for the MHD tests is shown in Figure 1. The generator consists of four basic parts. The first is the explosive driver. The explosive driver compresses argon gas to produce a plasma which is injected into the shock tube. The second component is the non-

conducting shock tube. The plasma shock front flows through this tube, interacting with the magnetic field to produce a voltage across the electrodes. The next portion of the generator is the magnetic field coils. The coils produce the magnetic field which gives rise to the charge separation. The transport of charge to the electrodes produces a voltage on the electrodes and thus current flow when the generator is connected to a load. The final portion of the generator experiment is the load itself. In all the tests reported, the load was reactive with a small resistive component.

The plasmas used in the MHD generators were produced using shock ionization of an argon gas. The explosive used in the experiments, Composition C-4, was packed into a driver which was shaped so as to optimize the plasma shock production. The explosive driver also acted to inject the plasma into the shock tube at high velocity. The explosive driver was not seeded to increase the ionization of the plasma. The time of arrival of the plasma was determined using shorting pins (called PINs in this report) as well as fiber optic probes. The PINs were small conducting pins placed along the shock tube in the plasma flow. A small bias voltage was placed on these PINs so that when they were broken by the arrival of the plasma front so that the measured signal change corresponds to the time of passage of the front at that location.

The field coils used in the experiments were driven by a capacitor bank that was protected from the effects of the explosive. The bank was charged and then switched to the coil by either single or multiple ignitrons. The coils produced fields ranging from 9 to 11.8 Tesla. The fields were uniform over the length of the electrodes in the interaction region. The field strengths were monitored using B-dot probes and the coil currents were monitored with Rogowski-type current probes.

The loads used in the tests were reactive with a small resistive component. The capacitors were connected to the generator electrodes using a short section of transmission line. For the low voltage experiments, the capacitors were mounted directly to the electrodes and shock tube by a strip line insulated with Kapton tape. In the high voltage tests, the load was shielded from the blast in a cement culvert with the electrical connection achieved using RG 220 cable. The load voltage was monitored using resistive dividers with the load current being measured using Rogowski coils.

5. LOW VOLTAGE GENERATOR

5.1 Overview

The components of the low voltage generator are shown in Figure 2. Many of the details of the first two years of the project that led to this design are described in two Sandia National Laboratories technical reports that contain the theory of operation, a discussion of the various components tested, modeling data, results, and the use of diagnostics on each test [12], [16].

The design reported here consisted of a 0.90 kg (2 lb.) explosive, cylindrical driver, and a 1.27 x 5.08 x 91.44 centimeter (0.5 x 2.0 x 36.0 inch) rectangular shock tube. The magnetic field was generated by an electromagnet consisting of two coils wound with Litz wire [13] placed on each side of the shock tube. The coil was energized with a 519 μ F capacitor bank which was then switched to the coils using an ignitron.

The load chosen for the low voltage generator tests consisted of four 2 μ F capacitors mounted on a parallel plate transmission line which provided a total inductance of 200 nH. The transmission line was insulated using Kapton tape to provide adequate voltage standoff. Figure 3 shows the equivalent circuit for the load. An overview of the experimental parameters for the low voltage tests is summarized in Table 1.

5.2 Pre-Shot Predictions

The performance of design #6 was predicted using the CTH hydrodynamics code. This code was used to determine the gas flow properties of the argon as it enters and propagates down the shock tube. With this approach the electromagnetics are ignored. The gas velocity U , gas density ρ , and the gas pressure P , were: $U = 25.5$ km/s, $\rho = 44.5$ kg/m³, and $P = 2.7 \times 10^8$ Pa or 2.7 kbars, respectively. These parameters resulted in a predicted open circuit voltage of 18 kV for a magnetic field of 14 T, using Equation (1) [13].

The load capacitors were modeled using the circuit analysis code Micro-Cap IV [17]. The circuit model designed to simulate the load with this generator design is shown in Figure 3. The results of Micro-Cap runs on this lumped circuit model are shown in Figure 4. The series of curves show the

variation of load voltage as the internal resistance of the generator is varied. Note that the variation is sensitive enough to allow an estimate of the internal resistance from the load characteristics.

5.3 Results

Diagnostics on the low voltage generator focused on the following generator parameters: plasma velocity measurements, magnetic field measurements, open circuit voltage, and eddy current plus the load voltage and current measurements. Since the electrode separation is known, the plasma velocity and magnetic field can be used to verify the open circuit voltage. The eddy current data provides an estimate of the magnetic Reynolds number given by:

$$R_m = \mu_0 \sigma U d, \quad (2)$$

where μ_0 is the permeability of free space, σ is the electrical conductivity, U is the plasma flow velocity, and d is the electrode separation distance. For the low voltage generator, the conductivity was estimated from the data from the plasma resistance probe.

The shorting pin data indicates a plasma velocity of 20 km/sec, 22% below the estimate. The maximum of the magnetic field was timed to coincide with the arrival of the plasma in the electrode region. The actual magnetic field measured was 9.4 T for the two shots. Using the given electrode separations, and actual measurements from the PIN data and B-dot probes, we now estimate an open circuit load voltage of 9.5 kV. The measured open circuit voltage was 31 kV for the first shot and 22 kV for the second shot, considerably higher than the simple estimate. From the data, the estimated plasma conductivity estimate was 18,400 Siemens/m, and the magnetic Reynolds number was 30.

As an example, Figure 5 shows the load voltage and current for the first shot. The maximum load voltage and current are 12.4 kV and 12.0 kA for this test. As indicated above, these values are more than a factor of two greater than those predicted on the basis of the plasma parameters and magnetic field given above. The higher measurement is probably due to the complications of geometry of the

electrodes and plasma flow resulting in Equation 1 providing only an order of magnitude estimate. However, this load voltage result is consistent with a matched load, being about one half of the open circuit value of 31 kV. When one compares the open circuit voltage trace with the load voltage trace there is evidence of electrical breakdown in both tests conducted with this generator design. In the case of test #1 (Figure 5) the breakdown occurs after the peak voltage is reached (see the discussion below).

5.4 Discussion

The plasma flow in the shock tube and the magnetic field coils behaved as expected. The results agree well with pre-shot testing and the predictions of code. However, from the load voltage traces on both tests, it is evident that electrical breakdown occurred. Nonetheless, peak values of voltage and a rough estimate of expected wave forms (without breakdown) can be made and compared to the generator open-circuit voltage measurements.

In the first low voltage experiment, premature breakdown apparently occurred in the transmission line section feeding the load (Figure 5). The fall-time of the load voltage is faster than the fall time of the open circuit voltage. This is presumably due to breakdown occurring between the two measurement points, i.e., in the feed to the load. Despite the breakdown in the feed, an estimate of the generator source impedance was obtained by matching the experimental voltage traces to a circuit model. The impedance obtained in this manner was 140 m Ω .

In the second test, breakdown again apparently occurred during the voltage pulse, this time in a cable used to connect the open circuit voltage probe to the MHD channel electrodes. Specifically, the failure likely occurred due to surface flashover in a Reynolds C cable connector. Subsequent laboratory tests of similar connectors indicated that failure occurred at 10 to 12 kV for a 100 ns applied pulse. Therefore it is doubtful that the measured open circuit voltage of 30 kV for several microseconds was held off by the connector. The breakdown of the open circuit voltage probe cable doubtless loaded the load voltage measurement. The measured load voltage peaked at approximately 4500 volts, which is about one-half that predicted for a perfectly matched load.

6. HIGH VOLTAGE GENERATOR

6.1 Overview

The generator used in the high voltage tests was a new design which employed a conical-shaped driver with an inverted cone inside specially configured to produce a fast plasma jet into the nozzle region that separated the driver section from the shock tube. The shock tube was much larger than the earlier design, but still rectangular in shape. Simple scaling predicts that the channel size of 1.27 x 30.5 x 91.4 cm (0.5 x 12.0 x 36.0 inches) has the capability of generating voltages exceeding 100 kV using magnetic fields comparable to those used in the low voltage tests. Figure 6 shows a drawing of the driver and shock tube.

The electromagnet required for the large generator was completely re-designed to fill a much larger volume with high magnetic field. A two-segment Bitter coil, consisting of a stack of ten 4130-steel plates (0.64 cm thick, 38 cm wide, 64 cm tall) which are welded together was used to generate the necessary magnetic field. The stack was connected by a copper bus-bar that allows for the fields generated by each side to be additive. The design goal was to provide a 14 T magnetic field in the center of a 7.62 cm by 33.0 cm rectangular region, requiring an energy of 2.5 MJ. The energy to drive the coil was supplied by a 3 MJ capacitor bank consisting six modules of 500 kJ each.

The reactive load used for this experiment consisted of three 50 kV, 1.34 μF capacitors connected in series. The total capacitance was 0.335 μF . This design was chosen based upon an equivalent circuit model as shown in Figure 7 and upon the ready availability of components. The load was connected to the generator electrodes using a 55.9 cm long section of the center conductor from RG 218 cable, contributing approximately 1 μH of series inductance to the load. The two sections of RG 218 center conductor are then connected through a small brass bus to RG 220 cable. The RG 220 cable extends for 23 meters to the capacitive load. The series inductance due to the RG 220 is 5.8 μH . Since the electrode region is immersed in the high magnetic field, the cable connections from the bus to the RG 218 were encased in a silicone-based adhesive and the entire region was enclosed in an SF_6 filled bag at standard temperature and pressure. The SF_6 was used to mitigate electrical breakdown. Two

Rogowski coils were used to determine the load current and two voltage dividers were used to monitor the load voltage.

6.2 Pre-Shot Predictions

For the high voltage experiment, the generator and shock tube design were based upon previous experience with other design tests. The gas pressure, plasma velocity, and plasma density were designed to be the same as in the low voltage generator tests. The design for the load circuit was based upon lumped circuit element models. The circuit model used for the high voltage generator and load is shown in Figure 7. Table 2 summarizes the key design features and predicted performance goals for the large MHD generator. Based upon the circuit model analysis of the experiment configuration, the expected load voltage waveform is shown in Figure 8. Since the load impedance is large, the variation of the voltage and current is minor and hence a family of curves is not shown.

6.3 Results

In the high voltage generator, the same diagnostics were utilized as in the low voltage experiments with the addition of an array of fiber optic probes. Since the separation of the probes along the shock tube is known, this diagnostic can be used to infer information concerning the plasma propagation through the shock tube. Figure 9 shows data obtained from the PIN's, indicating a plasma velocity of 7.5 km/sec. The peak magnetic field was 11.75 T at the time of arrival of the plasma front. These diagnostics indicate that the plasma flow velocity is a factor of four lower than expected, consistent with the reduced load voltage (from Equation 1). The pulse width is estimated to be 32 μ s. Figure 10 shows the load voltage and Figure 11 the load current. The peak voltage is 12 kV. This does not agree with initial pre-shot predictions which suggests a load voltage of 50 kV under matched conditions.

6.4 Discussion

The time-of-arrival data from the PINs is shown in Figure 9, and the two load voltage dividers and the load current Rogowski coil are shown in Figures 10 and 11. There is a great deal of ambiguity in the voltage data, however, along with the data from other diagnostics associated with this experiment, the following interpretation of the data has been formulated. The voltage signals prior to approximately 180 μ s are due to a plasma precursor shortly after the explosive driver is detonated (and the aluminum liner implosion begins). One explanation for this negative going voltage may be due to the fact that, at this point in time, the generator is essentially a linear Faraday generator, and as such appears as a capacitive circuit element.

The main plasma flow arrives in the electrode region at approximately 180 μ s, resulting in measured load voltage of 12 kV. This voltage, while much lower than desired, is consistent with the plasma flow being down by a factor of four, as described above. The large signal excursions late in time are likely due to ground loops induced as the experimental apparatus begins to move under the action of the high explosive detonation.

Two optical fibers were also used to obtain an estimate of the time of arrival of the plasma at positions along the shock tube. The position of the furthest upstream fiber was coincident with PIN #3, the second fiber was coincident with PIN #6, their axial separation being 15.24 cm. Each fiber's output was coupled into a monochromator tuned to 480.6 nm, a relatively strong line from Ar^+ .

Monochromator outputs were directly coupled into light detectors, light from furthest upstream being monitored by a Hamamatsu model R2658 photomultiplier and the second fiber output monitored by a fast semiconductor avalanche photodiode. Electrical signals from the detectors were fed into oscilloscopes that were triggered at the same time as the PIN detectors during the experiment.

The record from the photomultiplier is shown in Figure 12. Two features of this record should be noted: (i) a measurable optical signal begins at 20 μ s after trigger and continues to increase in intensity for 44 μ s at which time the photomultiplier saturates. (ii) There are three distinct slopes seen on the photomultiplier during the time interval 24 μ s - 65 μ s. The first feature suggests that plasma enters the shock tube gradually, perhaps not forming a well-defined shock front. It is easy to conjecture

that plasma forced through the rectangular aperture from the driver, which has cylindrical symmetry, would tend to spread out in some fashion as it fills the shock tube. The second feature allows an estimate of the plasma velocity. It is difficult to attach an arrival time for the plasma at the furthest upstream probe (photomultiplier), however it can be assumed that the steepest part of the signal (approximately the time of photomultiplier saturation) coincides with plasma arrival at 66 μs . Since the two fibers are separated by 15.24 cm these data give an average axial speed of 0.5 cm/ μs . It should be pointed out that the photomultiplier is capable of detecting very small light intensities. Although the monochromator is tuned to 480.6 nm the presence of a continuum of light which includes 480.6 nm could not be differentiated from a discrete source emitting at this wavelength. It is possible that the entire signal recorded from the photomultiplier is not solely due to singly ionized argon. This conjecture is supported by the spectroscopic data described below.

Data from the second fiber is shown in Figure 13. Tests prior to the experiment showed that the avalanche photodiode detector is not nearly as sensitive as the photomultiplier and requires relatively high intensity light to generate a significant electrical output. A weak signal may be seen on this record occurring at 96 μs . The later signals are attributable to breakup of the chamber and/or arrival of the hot gas from the explosion.

Four fibers provided separate optical signals from the experiment to an optical multichannel analyzer (OMA). These fibers were equally spaced by 5.08 cm (2.0 inches) with the furthest upstream fiber axial position coinciding with the upstream fiber discussed in the last section. The output of a 0.25-meter Czerny-Turner spectrograph, with a 600/mm line grating, was coupled to the detector of the OMA. The detector is a pulsed vidicon with a 500x500 array of cells. In anticipation of the presence of Ar^+ , the grating was tuned to place 480.6 nm near the middle of the observed spectral range. The signal from PIN #1 was used to trigger the OMA and an additional 3 μs delay added before the detector high-voltage pulse, which was 3 μs long. Figure 14 shows the spectra accumulated from the four fibers. These spectra are corrected for the wavelength-dependent response of the OMA by using an NIST standard lamp. The anticipated Ar II (Ar^+) line that should have been detected is at 4808 Å (480.8 nm). No evidence of Ar^+ is seen in these spectra which appear to be dominated by a continuum. It is

conceivable that the plasma temperature was sufficiently high to have "burned through" the first ionization state. It is well known that at temperatures exceeding 4-5 eV nearly all the argon will be in the second ionization state, which radiates predominantly in the ultraviolet. No attempt has been made to analyze the observed continuum; however it does not qualitatively resemble a blackbody spectrum.

Some useful information regarding the plasma velocity may be extracted when we consider that the OMA was triggered by the furthest upstream PIN (PIN#1). Plasma arrival at PIN#1 occurs at 63 μ s. When we include the 3 μ s delay for the OMA, spectroscopic data is accumulated over the time interval 66 μ s to 69 μ s. The first OMA fiber is located 7.62 cm downstream from PIN#1, the second 12.70 cm, the third 17.78 cm, and the fourth 22.86 cm. A barely measurable amount of light is seen at the third fiber position suggesting that the bulk of the plasma is still upstream of this position during the time data was acquired. During 6 μ s (3 μ s delay plus 3 μ s window) the plasma has at most traveled 13 cm, if the light observed by the OMA is due to the plasma. OMA data therefore indicates that the maximum axial velocity of the plasma is on the order of, or less than, 2 cm/ μ s. Absence of any argon lines, neither for singly ionized argon nor neutral argon, strongly suggests that the argon plasma has not yet arrived at any of the fibers monitored by the OMA. As noted before, it is difficult to imagine that the temperature of the plasma expanding through the shock tube aperture is in excess of 4-5 eV. If, in fact, the argon plasma has not yet arrived at the OMA fibers, the plasma cannot have an axial velocity in excess of 0.75 cm/ μ s.

The results of the high voltage generator test suggest several explanations for the poor generator performance. First, the poor vacuum in the shock tube may have contributed to the low shock front speed. The shock tube used for this test could not hold vacuum and leaked argon until the base pressure was reduced to 90 psi. However, it is not felt that this is the predominant reason for the poor performance [18]. Other explanations stem from the optical data. As suggested by this data, the plasma shock front expanded to fill the shock tube transverse to the direction of plasma flow. This expansion can only have come at the expense of the longitudinal shock front velocity. Further, another energy dissipation mechanism is suggested from the OMA data. In this interpretation, significant energy was

used for plasma heating, rather than kinetic energy of translation. Each of these effects can act to reduce the plasma velocity, thus reducing the voltage measured at the electrodes.

Another contributing factor may stem from the high magnetic Reynolds number of the plasma flow. This suggests that large boundary layers may have been induced along the walls of the shock tube impeding the current flow.

7. CONCLUSIONS

Two different designs for an explosively-driven MHD generator have been tested to determine their electrical behavior when delivering power to reactive loads. One of the original goals to develop the scaling of these generators as the shock tube size increases was not fulfilled. However, significant amounts of power were extracted from both designs.

The larger generator did not meet our expectations for voltage and power. This discrepancy can be attributed to several possible factors: i.) mismatch of the shock tube and driver, resulting in poor plasma flow, ii.) leaking of the vacuum and argon systems, iii.) the boundary layer problems resulting from a high Reynolds number.

All of the other objectives for the explosively-driven MHD pulsed power studies were successfully achieved. This included building experience in conducting explosive pulsed power tests, and setting up a compatible infrastructure. Also, the major objective of providing more training, equipment, and new procedures for operations when high voltage, explosives, and large support equipment like the capacitor banks were accomplished.

Further study of the generator designs is warranted for some HPM applications. In particular, the following steps should be taken before large scale MHD explosive testing is resumed:

1. Using a hydrodynamic code similar to CTH, conduct a study of the flow behavior of the large channel generator design. This will require 3D modeling, or 2D modeling using appropriate approximations near the throat of the tube. This study will be able to answer key questions regarding the effect of no initial vacuum in the shock tube so that a fuller understanding of the data from these experiments can be reached.

2. The code MACH2 [19] (and later MACH3 [20]) should be modified to allow for a complete analysis of the MHD characteristics of rectangular MHD generators that are explosively driven. The Hall effect, so important in MHD generators, must be included in the model.
3. Smaller scale laboratory experiments should be designed to study the issues associated with plasma boundary layer formation in a (height dominated) rectangular geometry. This would be the best way to verify the modeling results provided from following through with the recommendation above.
4. A way must be found to reduce the size and weight of the electromagnet needed for the 100 GW generator before this MHD generator designed is considered for employment with a compact HPM system. One concept would be to use a flux compression generator in concert with an MHD generator to provide the necessary magnetic flux during the time interval required.
5. These two designs demonstrated that the impedance of the MHD generator, while perhaps 100 times higher than an flux compression generator (approximately 200 m Ω versus 2 m Ω), is still lower than the tens to hundreds of ohms needed to match effectively with many HPM sources. Research on pulse conditioning must continue if compact HPM sources driven by explosive generators are to become a reality.

8. ACKNOWLEDGMENT

The authors would like to thank the entire Maxwell Laboratories, Inc. support contractors for their many hours of work to set up and help conduct these experiments. These tests would not have been possible without their help which many times exceeded their normal day-to-day operations and was never routine.

REFERENCES

1. H. E. Brandt, Alan Bromborsky, H. B. Bruns, and R. A. Kehs, "Microwave Generation in the Reflex Triode", Proceedings of the Second International Topical Conference on High Power Electron and Ion Beam Research and Technology, Ithica, NY, p 649, October, 1977.
2. G. Huttlin, M. Bushell, D. Conrad, D. Davis, K. Ebersole, D. Judy, P. Lezcano, M. Litz, N. Pereira, B. Ruth, D. Weidenheimer, and F. J. Agee, "The Reflex-Diode HPM Source on Aurora," IEEE Transactions on Plasma Science **18**, 618-625(1990).
3. A. D. Sakharov, "Magnetoimplosive Generators," Sov. Phys. Uspekhi (English Translation) **9**, 294-299 (1966).
4. J. W. Shearer et al, "Explosive-Driven Magnetic-Field Compression Generators," J. App. Phys. **39**, 2102-2116 (1968).
5. B. M. Novak, I. R. Smith, H. R. Stewardson, P. Senior, V. V. Vadher, and M. C. Enache, Design, construction and testing of explosive-driven helical generators," J. Phys. D: Appl. Phys. **28** 807-823 (1995).
6. J. Benford and J. Swegle, *High Power Microwaves*, Artech House, 1992, pp 160, 205, 206, 347.
7. I. R. Smith, B. M. Novac, and H. R. Stewardson, "Flux Compression Generators," IEE Engr. Sci. and Educ. J., 52-56 (1995).
8. M. Lehr, G. Baca, D. Chama, D. Schiffler, J. Graham, W. Sommars, and T. Englert, J. of Electronic Defense **20** No. 6, 45-47, 50 (June, 1997).
9. M. S. Jones, Jr. and C. N. McKinnon, Jr., "Explosive Driven Linear MHD Generators," Conference on Megagauss Magnetic Field Generation by Explosives and Related Experiments, H. Knoepfel and F. Herlack, (eds.), European Atomic Energy Community: Brussels, 1966, p. 349.
10. M. S. Jones, Jr. and V. H. Blackman, "Parametric Studies of Explosive Driven MHD Power Generators," MHD Electrical Generation, Vol. 2, 1964, p. 803.
11. S. P. Sharma, H. J. Schmidt, et. al., "Feasibility of an Optically Pumped Iodine Excimer .342 mm Laser Using Explosive MHD Generator Plasma," Megagauss Technology and Pulsed Power Applications," C. M. Fowler, R. S. Caird, and D. J. Erickson, (eds.), Plenum Press: New York, 1987, p. 757.
12. M. G. Vigil, B. D. Duggins, "Explosively-Driven Magnetohydrodynamic Generator: Phase I", Sandia National Laboratories, SAND94-0045, Aug. 1994.
13. F. J. Agee, F. M. Lehr, M. Vigil, R. Kaye, J. Gaudet, and D. Shiffler, "Explosively-Driven Magnetohydrodynamic (MHD) Generator Experiments", Digest of Technical Papers - 10th International Pulse Power Conference, W. Baker and G. Cooperstein, (eds), Albuquerque, NM, USA, July 3-6, 1995, pp 1068-1073.
14. J. M. McGlaun, S. L. Thompson, et. al., "A Brief Description of the Three-Dimensional Shock Wave Physics Code CTH", Sandia National Laboratories, SAND89-0607, 1990.
15. K. E. Shuler and J. B. Fenn (eds.), *Ionization in High-Temperature Gases*, Academic Press: New York, 1963.

16. M. G. Vigil, B. D. Duggins, "Diagnostics Instrumentation Systems Development: Explosively-Driven Magnetohydrodynamic Generator Project; Phase I," Sandia National Laboratories, SAND94-0046, February, 1994.
17. W. Steele, private communication. Spectrum Software, MicroCap IV 1021 S. Wolfe Rd., Sunnyvale, CA 94086 USA. Telephone: (408) 738-4387.
18. M. H. Frese, Numerex Corp., private communication.
19. M. H. Frese, "MACH2: A Two-Dimensional Magnetohydrodynamic Simulation Code for Complex Experimental Configurations," Mission Research Corporation Report AMRC-R-874, NTIS Doc, No. 192285 (1987).
20. U. Shumlak, T. W. Hussey, and R. E. Peterkin, Jr., "Three-Dimensional Magnetic Field Enhancement in a Liner Implosion System," IEEE Trans. on Plasma Sci. **23** No. 1 83 (1995).

Table I. Overview of the experimental parameters for the low voltage tests.

Explosive	COMP C-4, 2.0 lbs
Size of Shock Tube	0.5 x 2 x 36 inches, rectangular
Vacuum in Tube	~ 4 mTorr
Gas Driver	Argon at 200 psi
Magnetic Field Strength	9.4 T
Load Capacitance	8 μ F
Load Inductance	200 nH
Estimated Gas Velocity	25.5 km/s
Estimated Generator Open Circuit Voltage	12 kV
Estimated Power	2.3 GW

Table II. Key design features and predicted performance goals for the high voltage MHD generator.

Explosive	COMP C-4, 35.0 lbs
Size of Shock Tube	0.5 x 12 x 36 inches, rectangular
Vacuum in Tube	1 atm
Gas Driver	Argon at 90 psi
Magnetic Field Strength	11.4 T
Load Capacitance	0.335 μ F
Load Inductance	4 μ H
Estimated Gas Velocity	25.5 km/s
Estimated Generator Open Circuit Voltage	100 kV
Estimated Power	20 GW

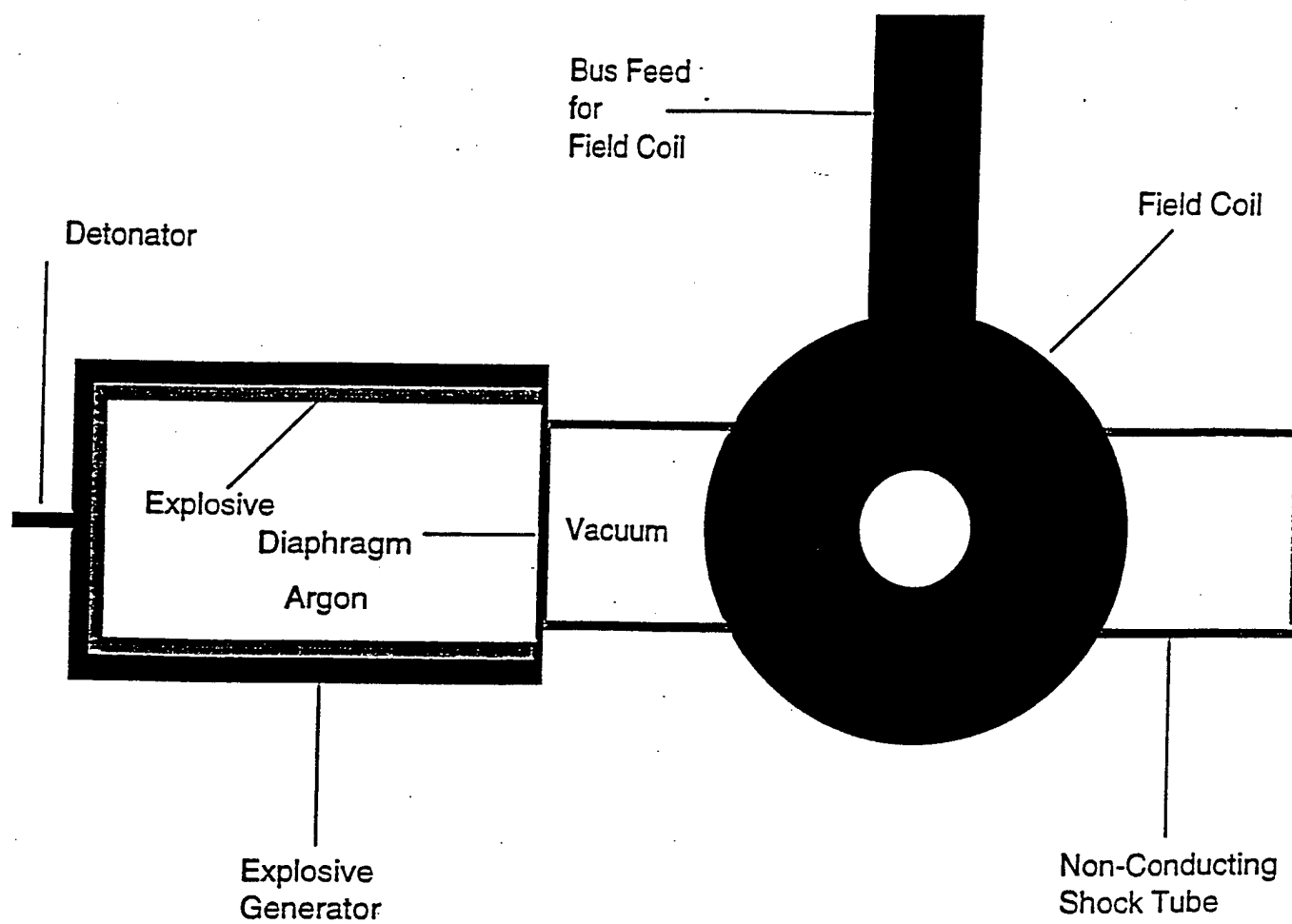


Figure 1. Generalized geometry for the MHD generator experiments. Each generator design shared these common features.

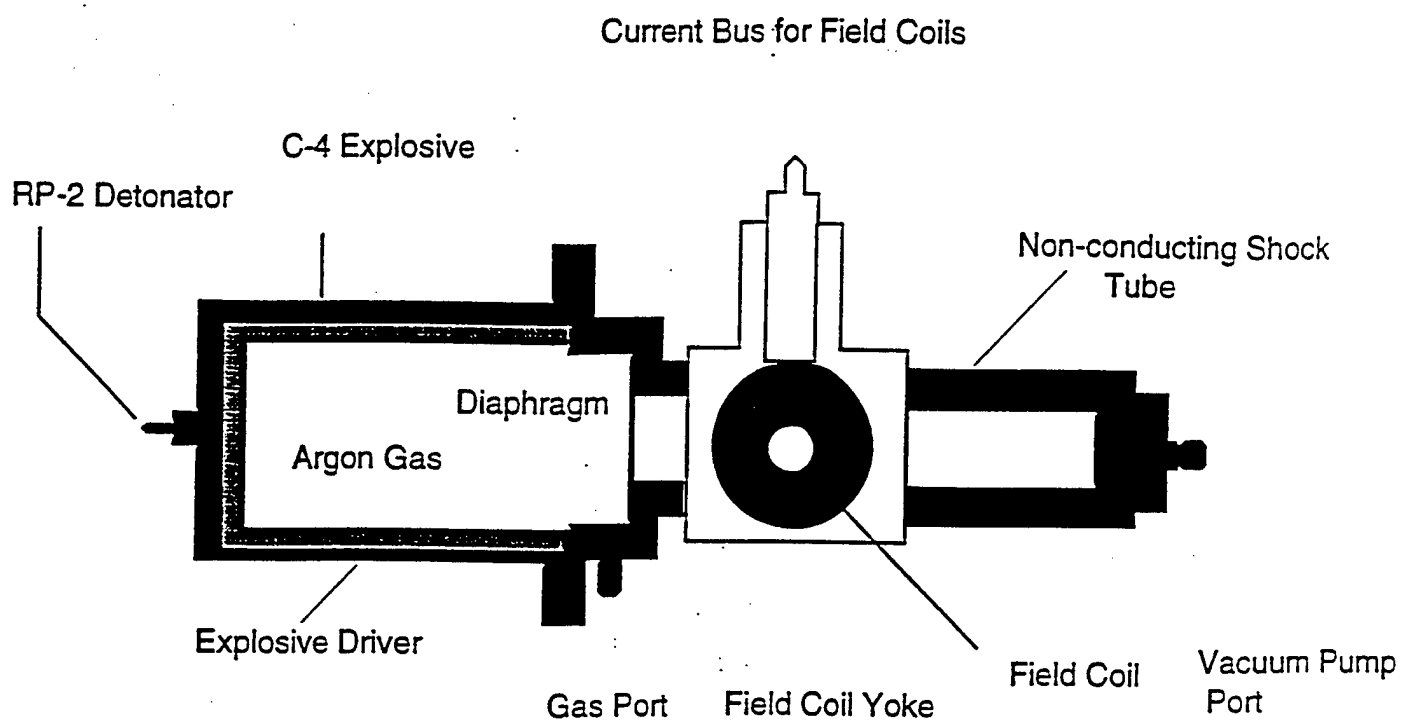


Figure 2. Schematic of the low voltage generator. The view shows basic components of the generator without showing the electrical load. The explosive is detonated with an RP-2 detonator. The magnetic field is produced using the coils depicted in the drawing.

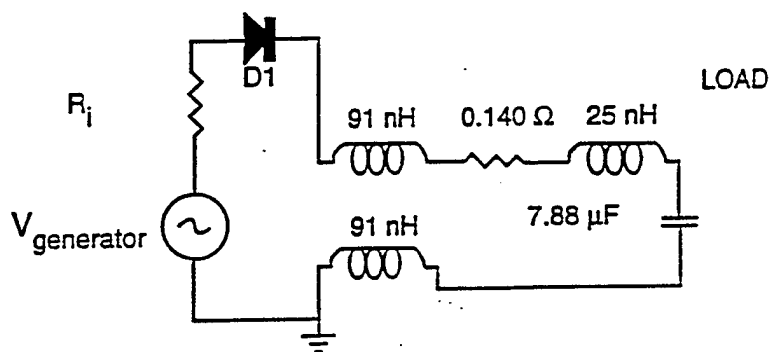


Figure 3. Equivalent circuit drawing for the generator and load used in the low voltage generator experiments. The resistance, R_i , is a variable parameter used to model the internal resistance of the generator.

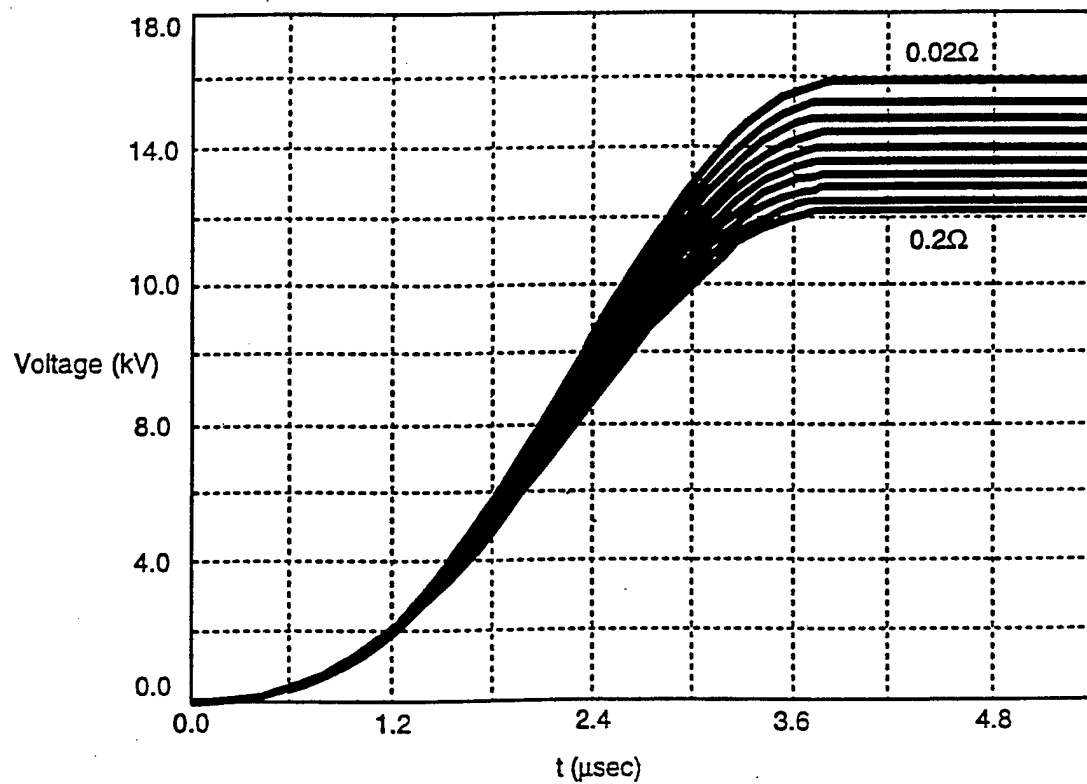


Figure 4. Results of the circuit simulation showing the load voltage as function of time for the low voltage generator. It shows a family of curves with the generator impedance as a free parameter.

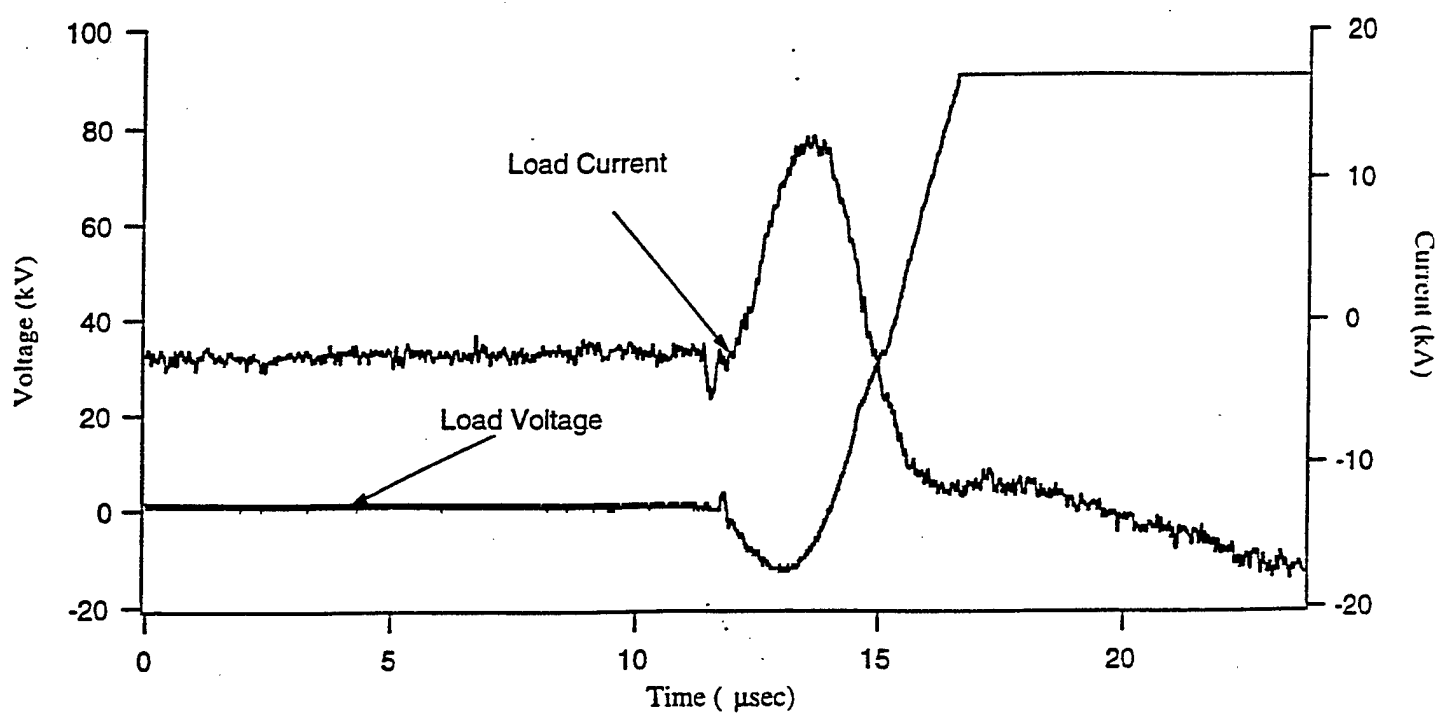


Figure 5. Load voltage and load current measured in the low voltage generator experiment, shot number 1. The peak voltage and current are 12.4 kV and 12.0 kA respectively.

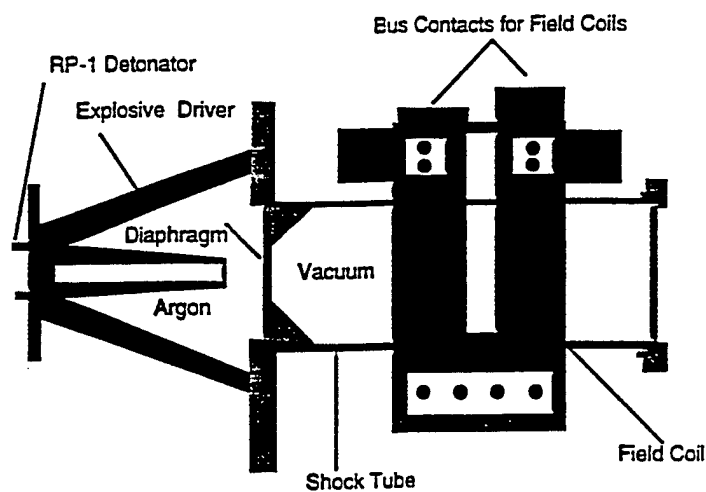


Figure 6. Schematic showing the design of the high voltage generator. Note the similarities to the low voltage generator shown in Figure 2. The major difference in the two generators is in the geometry of the explosive driver and the amount of explosives used in the experiment.

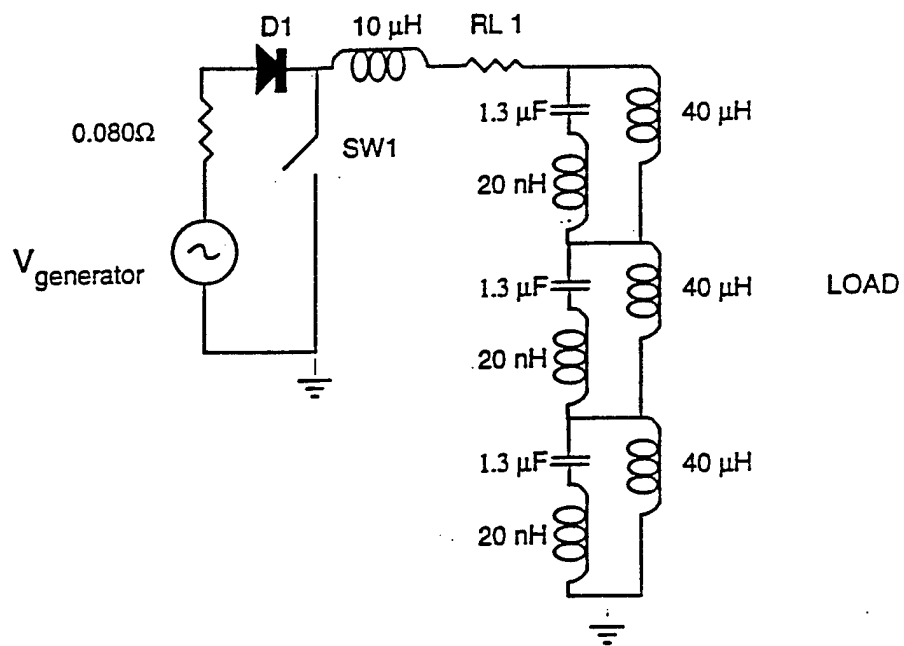


Figure 7. Equivalent circuit drawing for the generator and load used in the high voltage generator experiments.

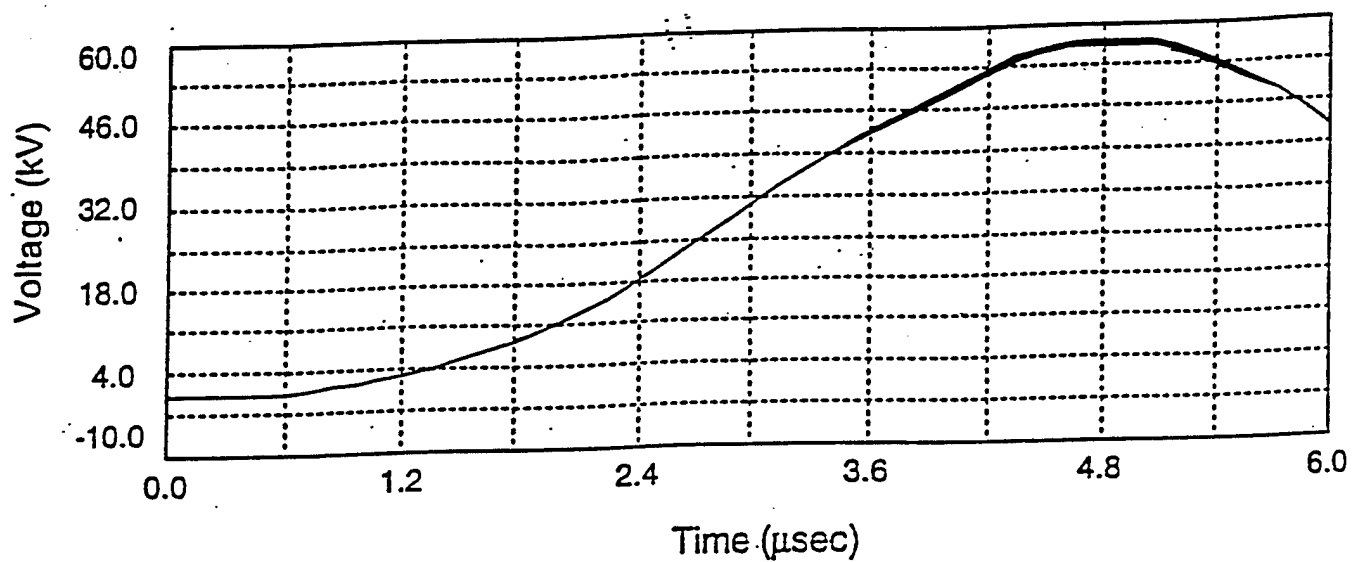


Figure 8. Predicted waveform for the load voltage in the high voltage generator experiment. Since the load impedance is large, the variation of the voltage and current is minor and hence a family of curves is not shown.

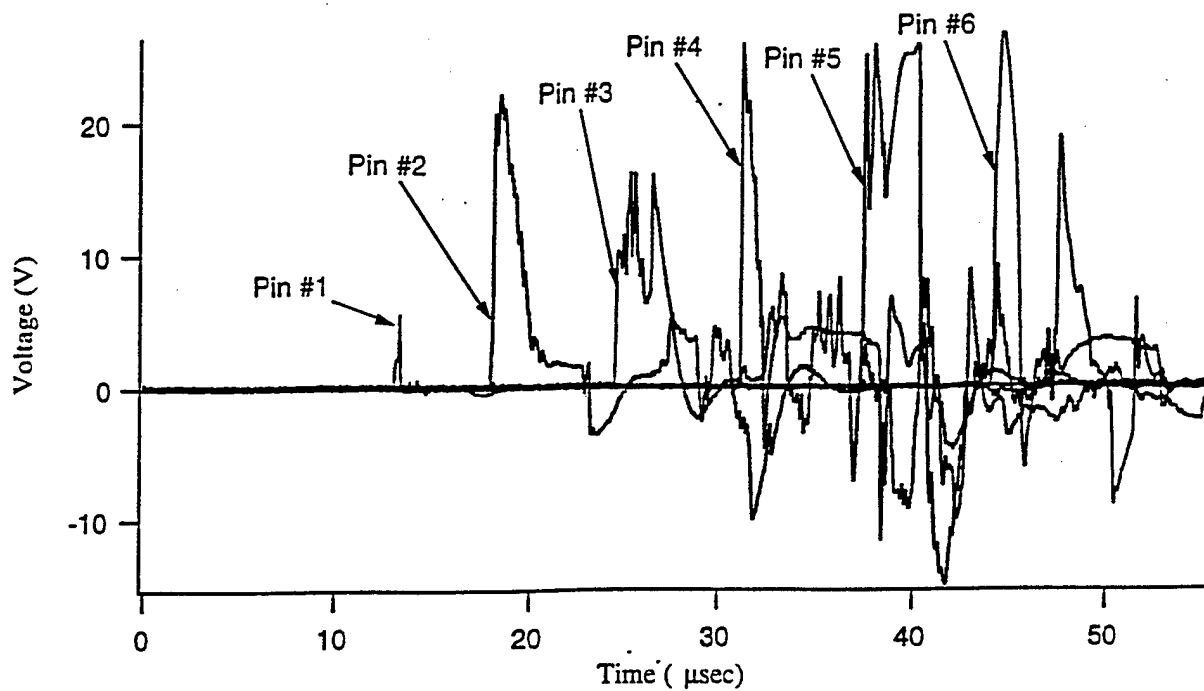


Figure 9. PIN signals from the high voltage generator experiments. The signals show the plasma arrival at various PIN positions along the shock tube.

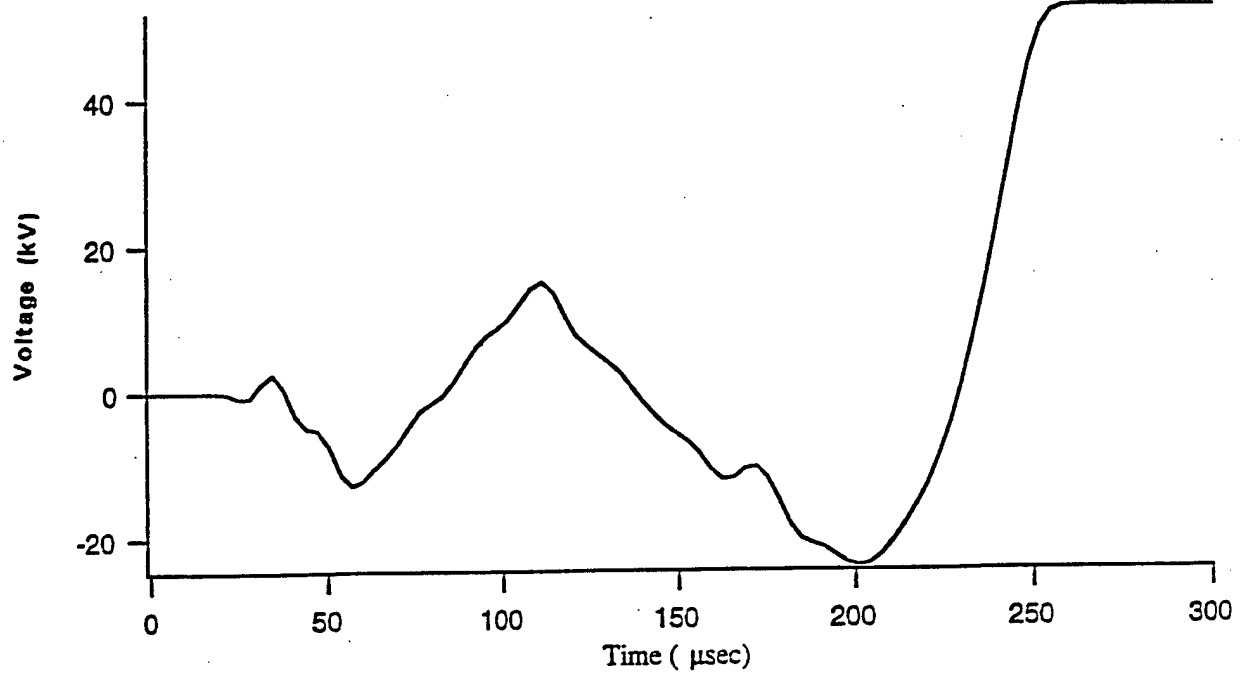


Figure 10. Load voltage measured in the high voltage generator experiment.

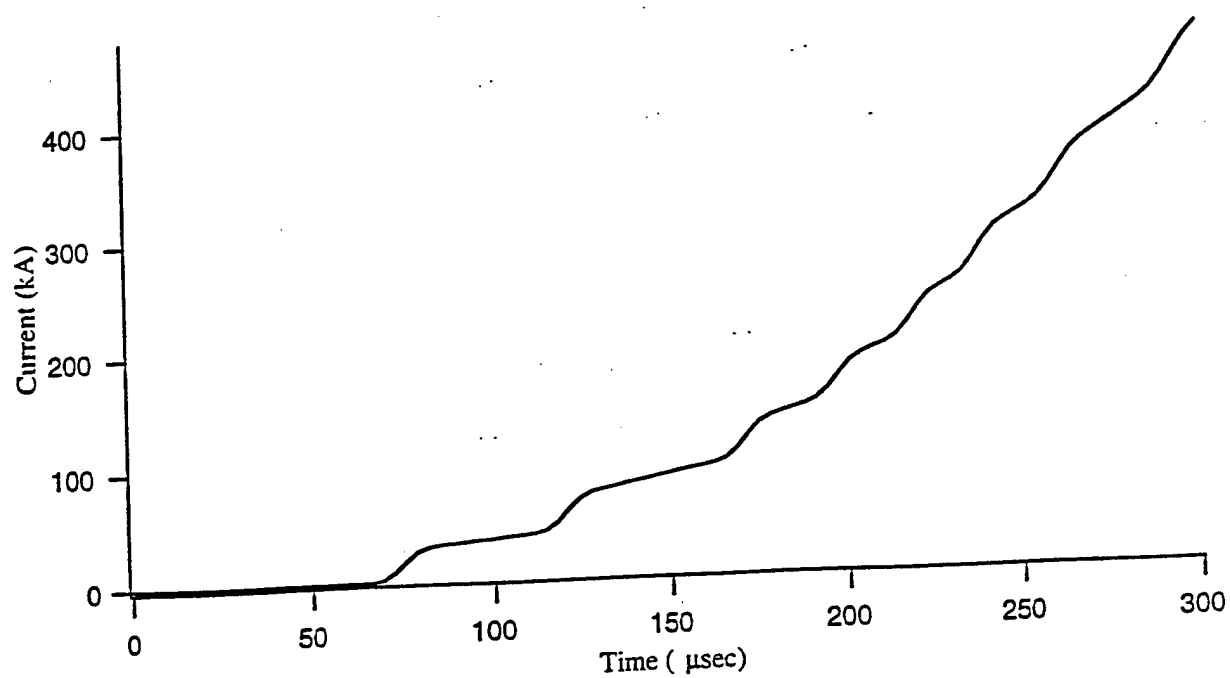


Figure 11. Load current measured in the high voltage generator experiment.

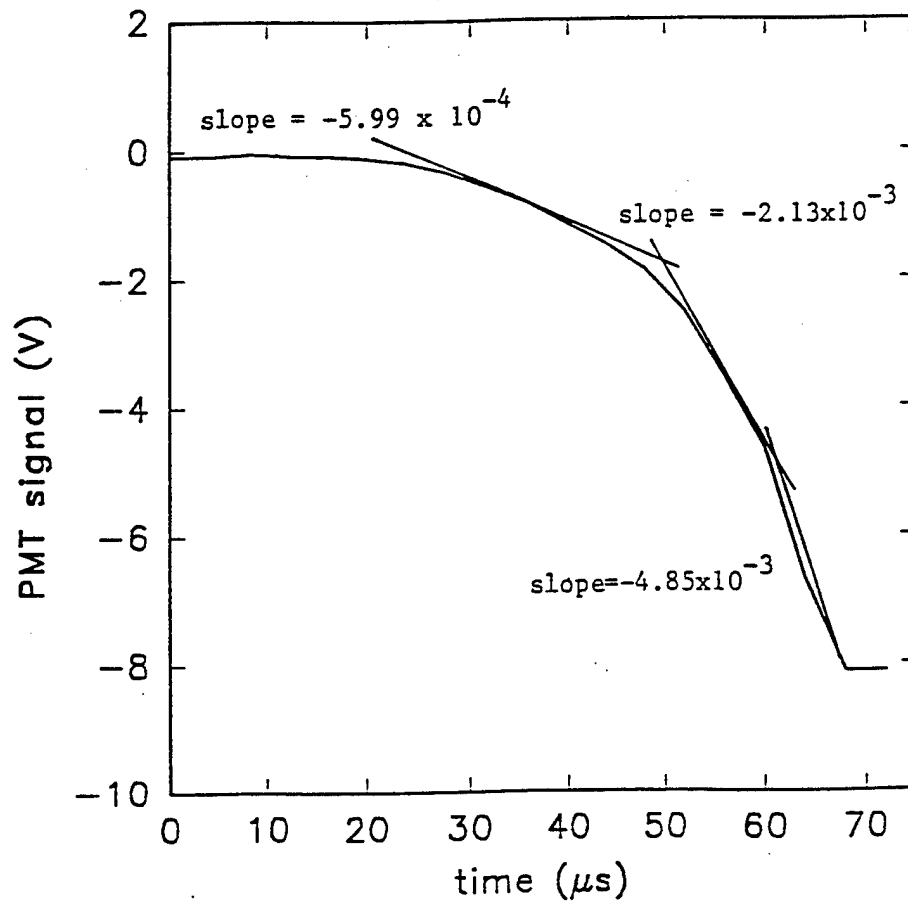


Figure 12. Signal from the first optical fiber used to determine the rate of plasma flow. Light is detected using a photomultiplier tube with a monochromator tuned to 480.6 nm. The different slopes seen on the curve indicate distinct changes in the plasma wave front.

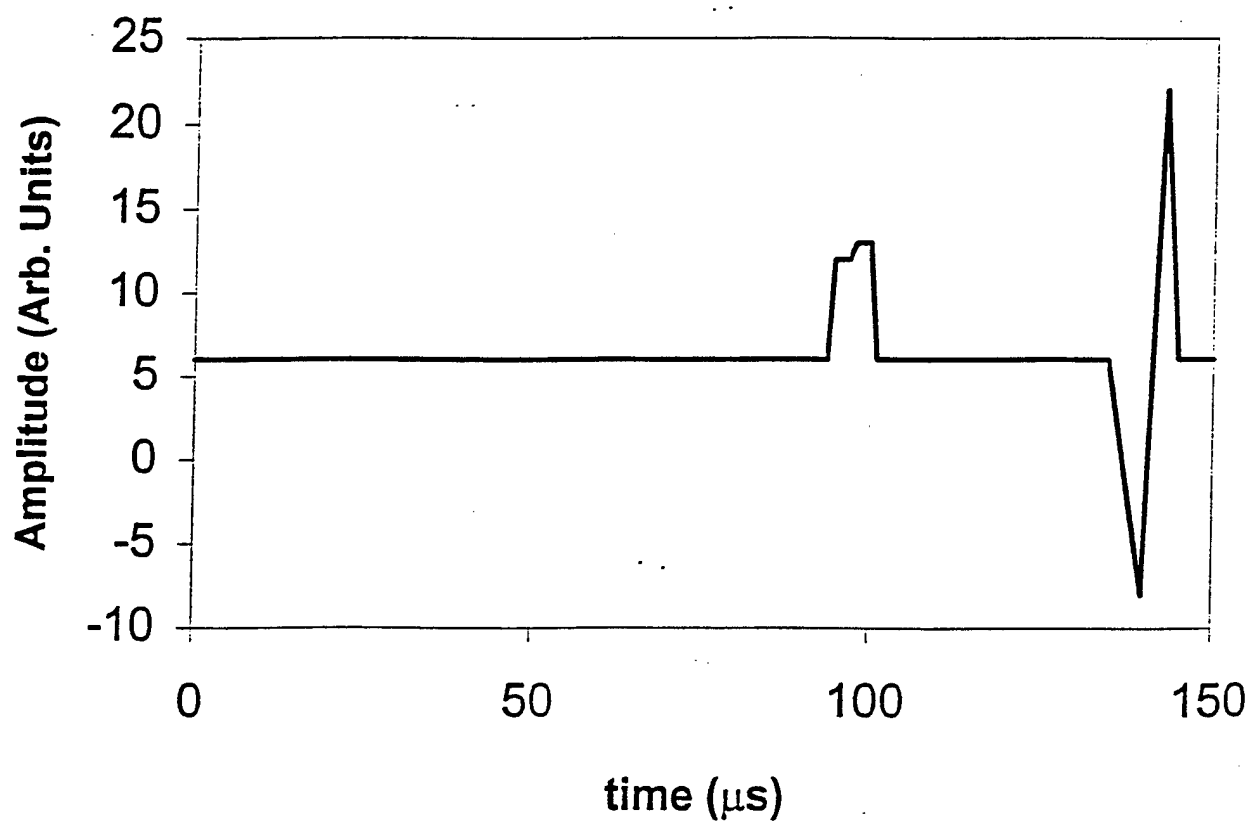


Figure 13. A re-plot of the data obtained from second optical fiber mounted along the shock tube. Average signal level is depicted. Light is detected using an avalanche photodiode coupled to a monochromator tuned to 480.6 nm. The probe position coincides with PIN #6.

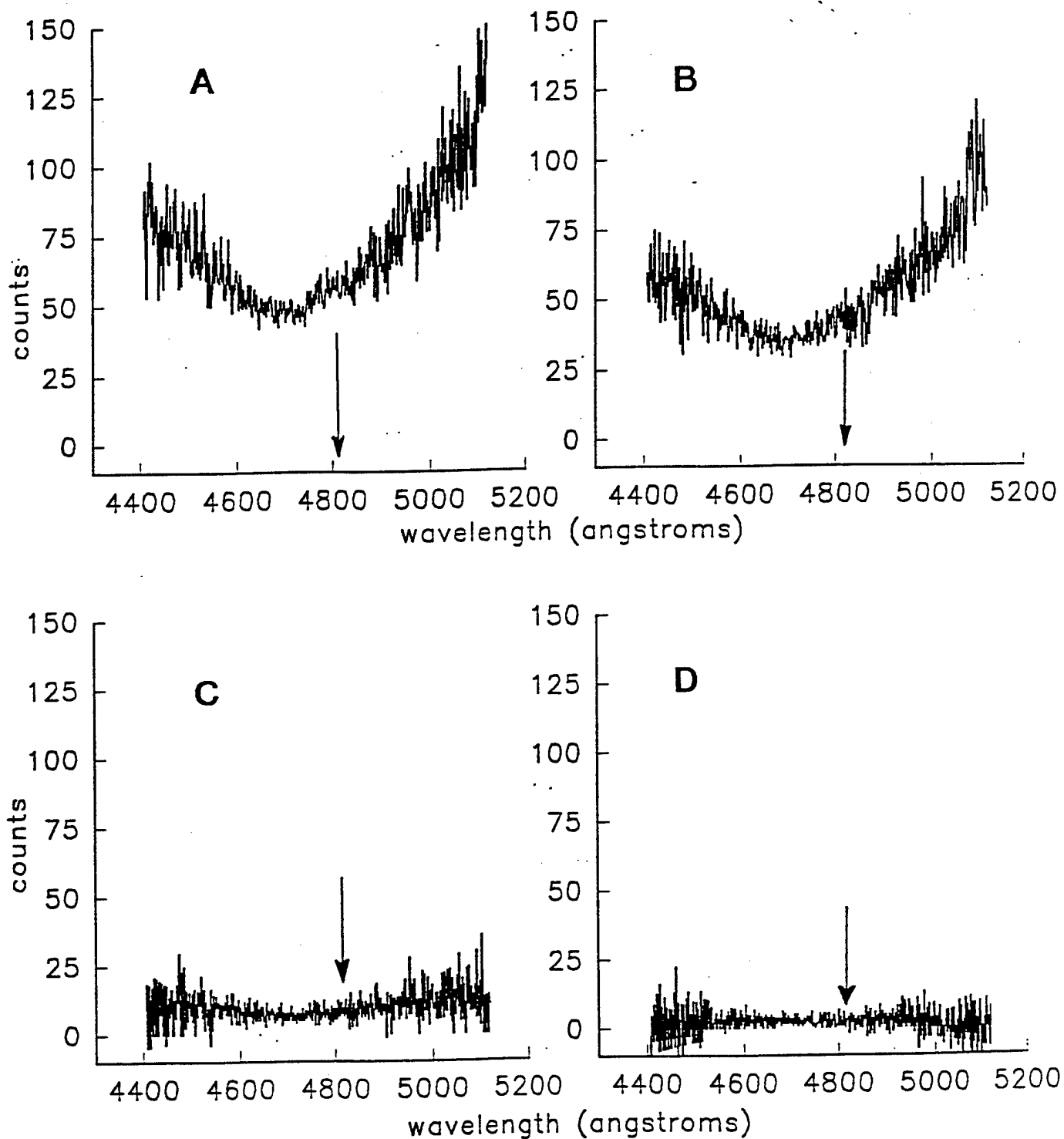


Figure 14. Optical spectra obtained from the plasma propagating along the shock tube. The fibers are placed in sequence, at A = 15.24 cm (6.0 in.), B = 20.32 cm (8.0 in.), C = 25.4 cm (10.0 in.), and D = 30.48 cm (12.0 in.), measured from the explosive driver side of the shock tube. Arrows indicate position of Ar II line at 480.8 nm.

DISTRIBUTION LIST

AUL/LSE Bldg 1405 - 600 Chennault Circle Maxwell AFB, AL 36112-6424	1 cy
DTIC/OCF 8725 John J. Kingman Rd, Suite 0944 Ft Belvoir, VA 22060-6218	2 cys
AFSAA/SAI 1580 Air Force Pentagon Washington, DC 20330-1580	1 cy
AFRL/PSTL Kirtland AFB, NM 87117-5776	2 cys
AFRL/PSTP Kirtland AFB, NM 87117-5776	1 cy
AFRL/DEHE ATTN: John Gaudet Kirtland AFB, NM 87117-5776	10 cys
Official Record Copy AFRL/DEHE/Leon J. Chandler	10 cys